IEEE Access
Multidisciplinary : Rapid Review : Open Access Journal

Received May 10, 2021, accepted June 14, 2021, date of publication June 28, 2021, date of current version July 21, 2021.

Digital Object Identifier 10.1109/ACCESS.2021.3092726

Doping-Less SiC p-i-n Diode: Design and Investigation

SARA HAHMADY AND STEPHEN BAYNE, (Senior Member, IEEE)
Department of Electrical Engineering, Texas Tech University, Lubbock, TX 79401, USA

Corresponding author: Sara Hahmady (sara.h@ttu.edu)

ABSTRACT We introduce a novel high-voltage SiC p-i-n diode considering a charge plasma approach. This technique facilitates the formation of the anode and the cathode regions within the silicon carbide without requiring any impurity doping by taking advantage of the work-function difference between silicon carbide and metal electrodes. Utilizing the 2-D TCAD simulation, we represent the performance of the proposed doping-less silicon carbide p-i-n diode is analogous to the silicon carbide Schottky diode in terms of forward and reverse characteristics as well as temperature dependency. As opposed to the conventional (doped) silicon carbide p-i-n diode, the doping-less silicon carbide p-i-n diode holds a lower ON-state voltage drop and higher reverse saturation current. Although the doping-less silicon carbide p-i-n diode has the merits of the silicon carbide Schottky diode, but it has leverage over the corresponding counterparts by eliminating the doping and the high thermal budget fabrication processes.

INDEX TERMS Charge plasma, doping-less, p-i-n diode, temperature dependency.

I. INTRODUCTION

Power rectifiers are required to regulate which direction the current flows in power electronic circuits. In a p-i-n diode, the depletion region supports the reverse-blocking voltage. Silicon carbide (SiC) based diodes have a considerably smaller drift region thickness and relatively higher doping concentration in comparison with silicon-based devices, which lead to the designing of 4H-SiC diodes and achieving higher breakdown voltages [1].

Since Schottky diodes have a faster switching response in contrast to p-i-n diodes, the SiC Schottky diodes could replace p-i-n diodes in power applications with blocking voltage up to 3000 V with lesser ON-state voltage drop. This transformation demands further advancement with lowering the cost and complexity of SiC technologies [1].

In situ n-type and p-type doping during the epitaxy process of the SiC which is done through the Chemical Vapor Deposition (CVD) is quite robust these days and at the same time it is very complicated, highly depends on pressure, and requires reactors with a high temperature of 1550° C. In SiC, diffusion constants of dopant impurities are extremely small due to strong chemical bonding, even at temperatures as high as 1800° C. Therefore, ion implantation is used for selective doping of SiC at the cost of more lattice damage and expensive process [2].

To overcome these intricate and expensive processes mentioned earlier an innovative doping-less SiC p-i-n diode is proposed using the charge plasma concept. There are numerous studies and research on different semiconductor devices considering the charge plasma concept and creating doping-less (junction-less) devices. Nanoscale p-n diode was a primary device that is designed and fabricated applying this technique [3]–[5]. Doping-less bipolar transistors (BJTs), Schottky collector bipolar transistor without impurity doped emitter and base [6]–[9], laterally singled-diffused metal oxide semiconductor, Junction-less Impact Ionization MOS, Doping-less tunnel field effect transistor and high voltage devices such as strained super-junction vertical single diffused MOSFET, silicon-based 50 V p-i-n diode [10]–[22] are designed utilizing charge plasma concept which not only reduces the process of fabrication, but in some cases results in a better performance as compared with the conventional (doped) counterparts.

In this study, for the first time, a 4200 V SiC p-i-n diode is designed without demanding high-temperature diffusion, ion implantation, or annealing procedures. The P anode and N cathode are induced in the silicon carbide by

The associate editor coordinating the review of this manuscript and approving it for publication was Tuo-Hung Hou.

This work is licensed under a Creative Commons Attribution-NonCommercial-NoDerivatives 4.0 License.
For more information, see https://creativecommons.org/licenses/by-nc-nd/4.0/

selecting the appropriate anode and cathode metal electrodes with work-functions greater than SiC and less than SiC respectively.

Using TCAD 2D-simulations [23], we demonstrate a detailed comparison of the I-V characteristics and temperature dependency of the proposed doping-less SiC p-i-n diode under forward and reverse bias, with SiC Schottky diode and doped (conventional) SiC p-i-n diode.

II. STRUCTURES AND SIMULATION PARAMETERS

Fig. 1. shows the cross-sectional view of the parallel plane doped SiC p-i-n diode, SiC Schottky diode, and the proposed doping-less SiC p-i-n diode. The conventional parallel plane p-i-n diode and Schottky diode are designed for a blocking voltage of 3300 V. Since the blocking voltage is typically 80% of the actual breakdown voltage, the diode is designed for a breakdown voltage of 4200 V [24]. considering the 4200 V breakdown voltage ($V_{BD} = 4200\ V$) for power application, the dielectric constant of SiC (ϵ_{SiC}), electron charge (q), with the drift region width of $t_{drift} = 30\ \mu m$, the corresponding doping concentration of drift region can be derived [2]:

$$N_{drift} = \frac{2.\epsilon_{SiC}.V_{BD}}{q.t_{Drift}{}^2} = 3.8e15\ \ cm^{-3} \qquad (1)$$

Fig. 1(a) illustrates the cross-sectional view of the doped p-i-n diode and, P anode and N cathode represent the evenly doped regions. In this structure, aluminum is assumed to be the p-type dopant while nitrogen is the n-type dopant. P_{CP} anode region and N cathode region in Fig. 1(b) represent the induced positive charges because of the Schottky contact and uniform n-type doped region by nitrogen dopant in Schottky diode respectively.

In the doping-less p-i-n diode shown in Fig. 1(c), the N_{CP} cathode region represents the negative charges induced by the cathode Schottky contact and, the P_{CP} anode region illustrates the induced positive charges as a result of an appropriate anode Schottky contact. Throughout this study, to create N_{CP}, two different contact with work-functions of 3.9 eV and 3.5 eV are selected as the cathode contact. To generate P_{CP}, and to observe the influence of the anode work-function on the characteristics of doping-less p-i-n diode and Schottky diode, two different electrode work-functions of 5.4 eV and 5.65 eV, are considered as the anode contact [24]. Electron and hole lifetimes are selected to be 3.33 μs and 0.67 μs respectively [2], [23], [24].

The Debye length $L_D = [(\epsilon_{SiC} \cdot \upsilon_t) / (q \cdot N)]^{1/2}$ (ϵ_{SiC} is the dielectric constant of SiC, υ_t is the thermal voltage, and N is the carrier concentration), is the distance at which the induced carrier concentration maintains uniform distribution in the SiC at the Schottky contact/SiC interface [3] and since this distance is measured to be in nanometers, the t_{drift} of 30 μm will be the entire SiC doping-less p-i-n diode.

Simulation specifications are mentioned in Table 1. The models considered for our simulations are Shockley-Read-Hall recombination (SRH), Fermi-Dirac statistics (FERMI), auger recombination (AUGER), bandgap narrowing (BGN), low field mobility (ANALYTIC), carrier-carrier scattering (CONWELL), impact ionization(IMPACT SELB),

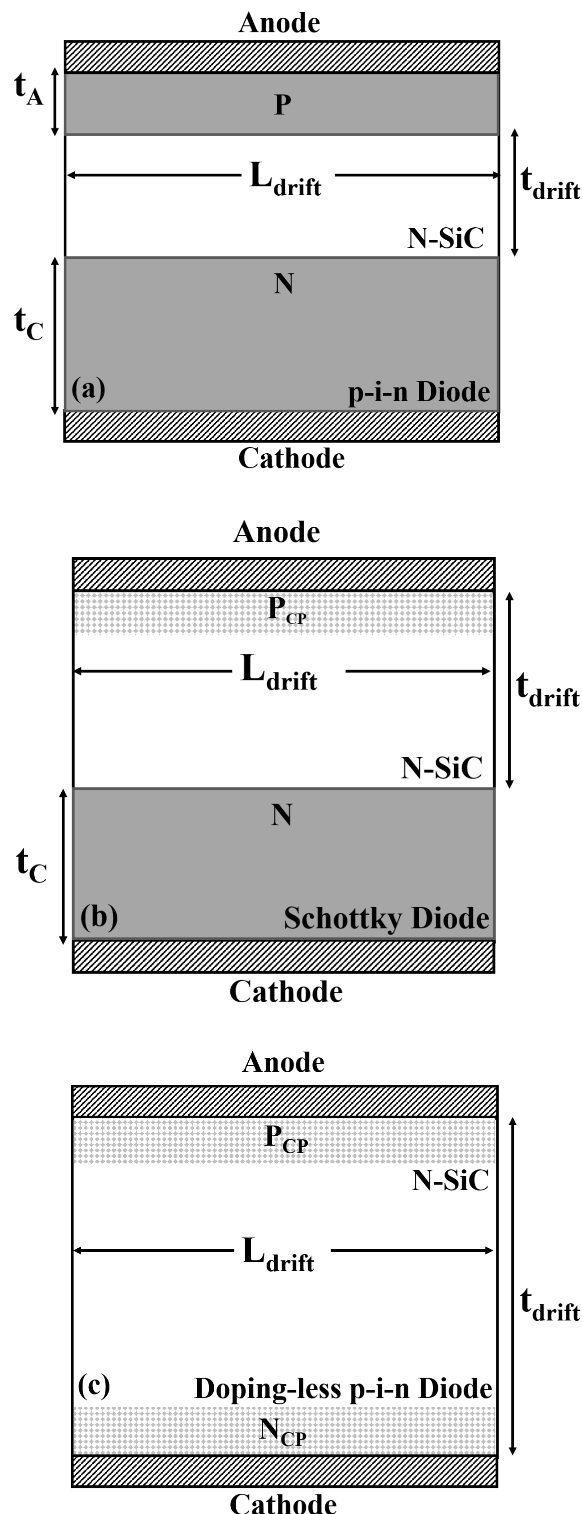

FIGURE 1. Schematic cross-sectional view of (a) The parallel plane doped SiC p-i-n diode. (b) The parallel plane SiC Schottky diode. (c) The Proposed doping-less SiC p-i-n diode.

TABLE 1. Simulation specifications.

-	p-i-n	Schottky	doping-less p-i-n
t_A μm	2	-	-
t_C μm	150	150	-
t_{drift} μm	30	30	30
L_{drift} μm	10	10	10
P cm^{-3}	1e21	-	-
N cm^{-3}	1e20	1e20	-
N_{drift} cm^{-3}	3.8e15	3.8e15	3.8e15

Parabolic Field Emission (PARABOLIC), thermionic emission (THERMION), barrier lowering (BARRIER), lattice temperature (LAT.TEMP), and temperature model (TEMP).

III. RESULTS AND DISCUSSION

A. FORWARD AND REVERSE CHARACTERISTICS

Fig. 2 illustrates the electron and hole concentration of the conventional SiC p-i-n diode, Schottky diode and doping-less SiC p-i-n diode under zero bias along the vertical cut-line from anode region to the cathode side. Fig. 2(a) shows the electron and hole concentration of the conventional doped p-i-n diode. The $2\mu m$ thick P region on the left side of the Fig. 2(a), and $150\mu m$ thick N region on the right side of the graph, represent anode and cathode doped regions respectively.

The carrier concentration of the Schottky diode for two different anode work-function is represented in Fig. 2(b). By considering contacts with the work-functions of 5.65 eV and 5.4 eV being the anode contact in Schottky diode, the induced positive charges, P_{CP}, are formed at the SiC/anode metal interface in the SiC.

Fig. 2(c) indicates the carrier concentration within the doping-less SiC p-i-n diode under equilibrium condition. Each anode and cathode contact has two different work-functions. The anode contact has two work-functions of 5.65 eV and 5.4 eV, while the cathode contact has two work-functions of 3.5 eV and 3.9 eV.

As Fig. 2(c) depicts, since anode contact has a higher work-function than SiC, electrons move from SiC interface into contact which leave positive charges (P_{CP}) behind (at left side of the graph). On the other hand, because cathode contact has a lower work-function compare to SiC, electrons move to the SiC and create negative charges (N_{CP}) at the interface (at the right side of the graph). It is clear that value of the work-function defines the amount of the induced positive and negative charges at the interface. Higher the work-function difference between contacts and semiconductor, the higher the induced carrier concentration will be.

Fig. 3 illustrates the energy band diagram of the doping-less p-i-n diode under equilibrium condition for the two different work-functions. At the anode/SiC interface, presence of the induced positive charges (P_{CP}) discussed in Fig. 2(c), leads to bending of the conduction band upward. On the contrary, at the SiC/cathode interface, due to the existence of the induced negative charges (N_{CP}) explained in Fig. 2(c), the conduction band bends downward at the interface.

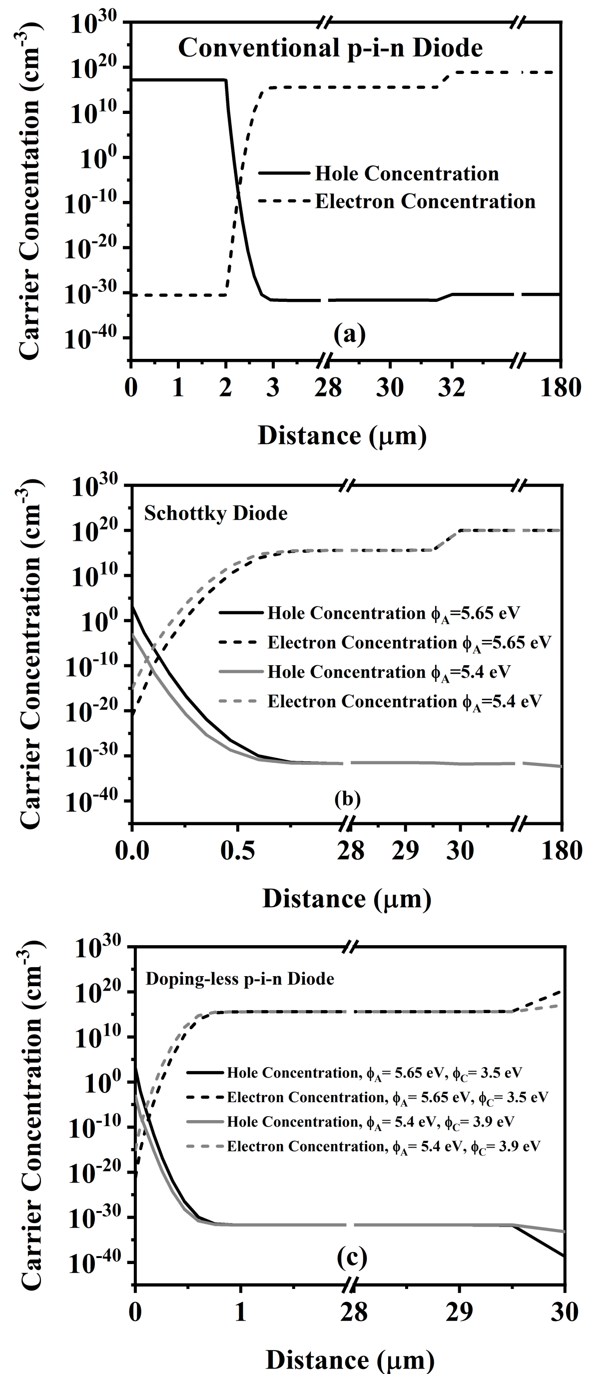

FIGURE 2. Electrons and holes concentration along a vertical cut-lines under equilibrium (a) The doped p-i-n diode. (b) The Schottky diode. (c) The doping-less p-i-n diode.

Fig. 4, shows forward I-V characteristics of the conventional p-i-n diode, Schottky diode and doping-less p-i-n diode. In the SiC Schottky diode and doping-less SiC p-i-n diode, the current across Schottky contacts and semiconductor junctions is mainly because of the presence of the majority carriers. Although there are multiple current

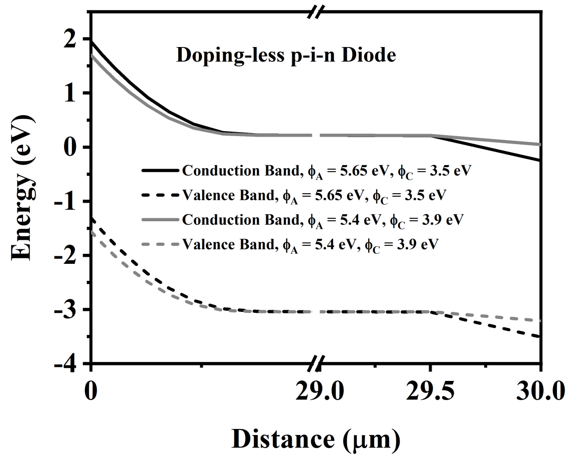

FIGURE 3. Energy band diagram of the doping-less p-i-n diode under equilibrium with two different work-functions of 5.65 *eV* and 5.4 *eV* as anode contact; And two different work-functions of 3.5 *eV* and 3.9 *eV* as cathode contact.

mechanisms such as tunneling and recombination, prior studies have shown that the thermionic emission is the leading mechanism in Schottky contact and semiconductor junctions [1], [15], [25]. Therefore, as Fig. 4(a) shows the doping-less p-i-n diode and Schottky diode have approximately indistinguishable linear forward characteristics for two different work-functions of 5.4 eV and 5.65 eV due to similar forward thermionic current mechanism. As Fig. 4(a) indicates, the Schottky diode and the doping-less p-i-n diode have the ON-state voltage drop of 1.8 V and 2.1 V at the forward current density of 100 A/cm^2 for two different work-function of 5.4 eV and 5.65 eV respectively.

Fig. 4(b) and Fig. 4(c) depict the linear and semi-log forward characteristics of the doping-less p-i-n diode and doped p-i-n diode, respectively. In the doped p-i-n diode, at low forward voltages, the recombination of carriers in the space-charge region controls the current. By increasing the voltage, minority carriers start to diffuse into the drift region and, at this point the concentration of these minority carriers is far below the background doping. Therefore, the low-level injection current dominates the forward current. Increasing the voltage further gives rise to the number of injected minority carriers beyond the doping concentration of the drift region. Under these circumstances, the high-level injection current leads the forward current [25]. As we mentioned earlier, the leading determinant in the current mechanism of the doping-less p-i-n diode and Schottky diode is the thermionic emission of the majority carriers over a potential barrier [15], [25], while diffusion of the minority carriers is the deciding factor in the doped p-i-n diode [1]. Consequently, due to this difference, as shown in Fig. 4(b) and Fig. 4(c), the ON-state voltage drop of the doped p-i-n diode at the forward current density of 100 A/cm^2, is almost 1.4 V and 1.1 V higher than the doping-less p-i-n diode with the anode contact work-function of 5.4 eV and 5.65 eV respectively [15]. Fig. 4. indicates how an appropriate low barrier height and forward voltage bias

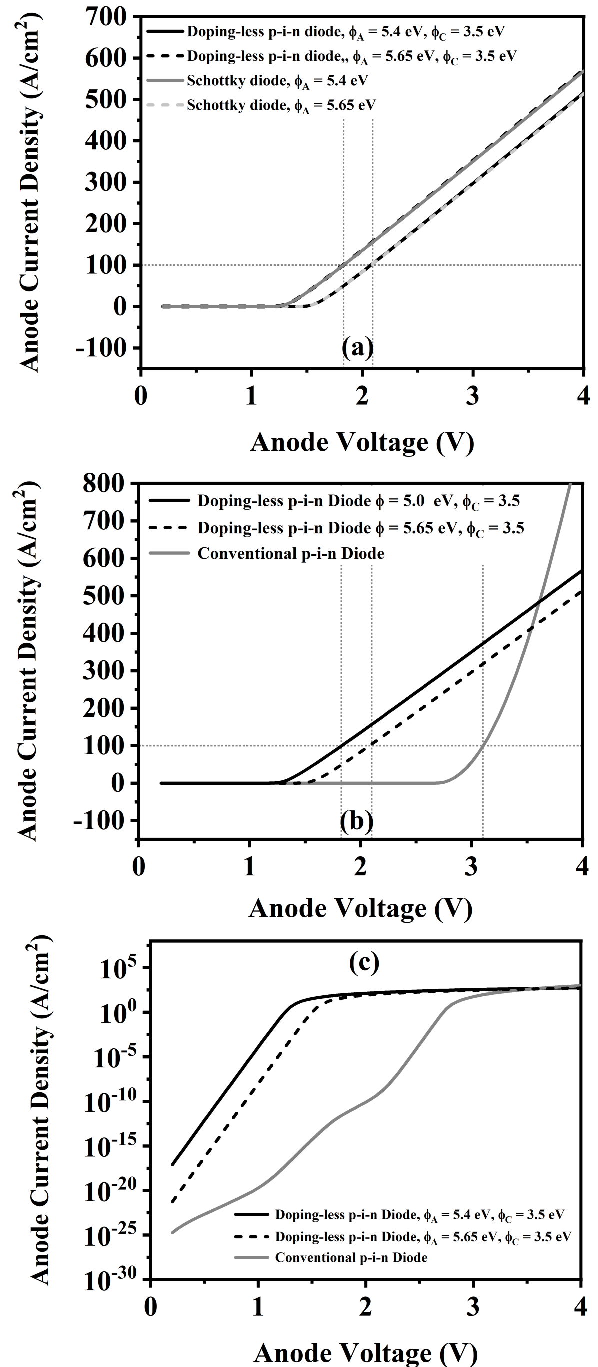

FIGURE 4. (a) Forward I-V characteristics of the doping-less p-i-n diode and Schottky diode for two different anode metal contacts with work-functions of 5.4 *eV* and 5.65 *eV* with cathode metal contact with work-function of 3.5 *eV* on linear scale. (b) Linear scale of forward I-V characteristics of the doping-less p-i-n diode and Schottky diode for two different anode metal work-functions of 5.4 *eV* and 5.65 *eV* with cathode metal work-function of 3.5 *eV* and conventional doped p-i-n diode. (c) Semi-log forward I-V characteristics of the doped p-i-n diode and doping-less p-i-n diode for two different metal work-functions of 5.4 *eV* and 5.65 *eV* as the anode metal with cathode metal work-function of 3.5 *eV*.

facilitates the injection of carriers through the barrier, leading to a higher forward-bias current across the devices and lower ON-state voltage drop.

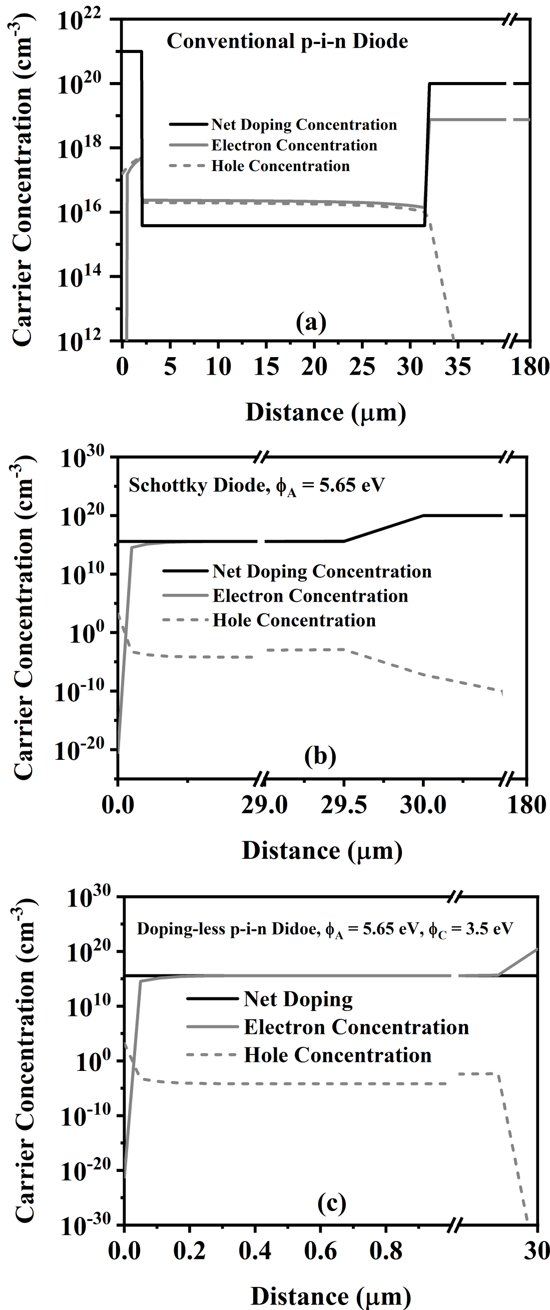

FIGURE 5. Carrier concentration along a vertical cut-lines under On-state forward bias of (a) The doped p-i-n diode (b) The Schottky diode (c) The doping-less p-i-n diode.

Fig. 5 shows the carrier concentration of the doped SiC p-i-n diode, SiC Schottky diode, and doping-less SiC p-i-n diode along the vertical cut-line across the drift regions during On-state forward bias.

Fig. 5(a) indicates the high-level injection of the minority carriers within the drift region of the doped p-i-n diode requires an equal concentration of electrons, as per charge neutrality. This high concentration of the free carriers, which exceeding the background doping of the drift region, results in a drastic reduction of ON-resistance of the diode known as conductivity modulation. Under the high-level injection regime, the operation current density is in the range of $100\ A/cm^2$ to $200\ A/cm^2$.

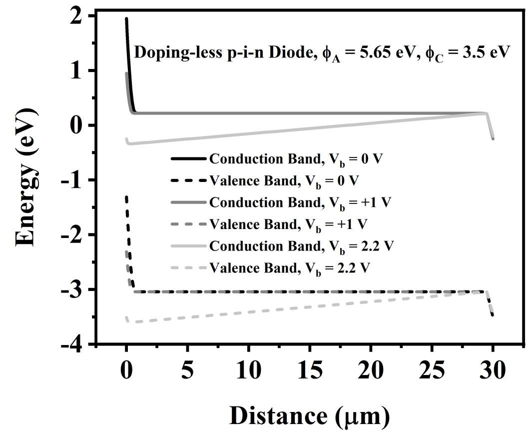

FIGURE 6. Energy band diagram of the doping-less p-i-n diode for three different voltage biases of: 0 *V*, 1 *V* and 2.2 *V*.

Increasing the forward current density beyond the high-level injection current forces the minority carriers into the heavily doped end regions besides the drift region. Consequently, the overall current density of the p-i-n diode consists of the recombination current of the minority carriers in the end regions and the drift region. Once the forward current density surpasses $100\ A/cm^2$, the ON-state voltage drop rises significantly due to the end region resistance effect [24], [25].

Considering the fundamental difference between these current mechanisms mentioned earlier, contrary to the doped p-i-n diode, the carrier concentration of the Schottky diode and doping-less p-i-n diode do not exceed the background doping of the drift region, as represented in Fig. 5(b) and Fig. 5(c).

The concept of the charge plasma and consequently the doping-less p-i-n diode is based on the work-function difference between the contacts and semiconductors. Fig. 6 demonstrates the band diagram across the doping-less p-i-n diode along the vertical cut-line from anode contact to cathode contact under equilibrium, 1.0 V and 2.2 V forward biases.

As the forward bias is applied the barrier height at the anode side decreases while the bands at the cathode side remains uninterrupted. As the forward voltages increases the barrier height decreases which leads to higher forward current density.

Fig. 7(a) depicts the semi-log reverse characteristics of the doping-less p-i-n diode and the Schottky diode with two different work-function of 5.4 eV and 5.65 eV. Leakage current in the Schottky diode, as well as doping-less p-i-n diode comprises of several current mechanisms such as, generation-recombination current and reverse-bias hole diffusion current. However, thermionic emission is the primary mechanism responsible for the leakage current [24]. In the conventional p-i-n diode the space-charge generation

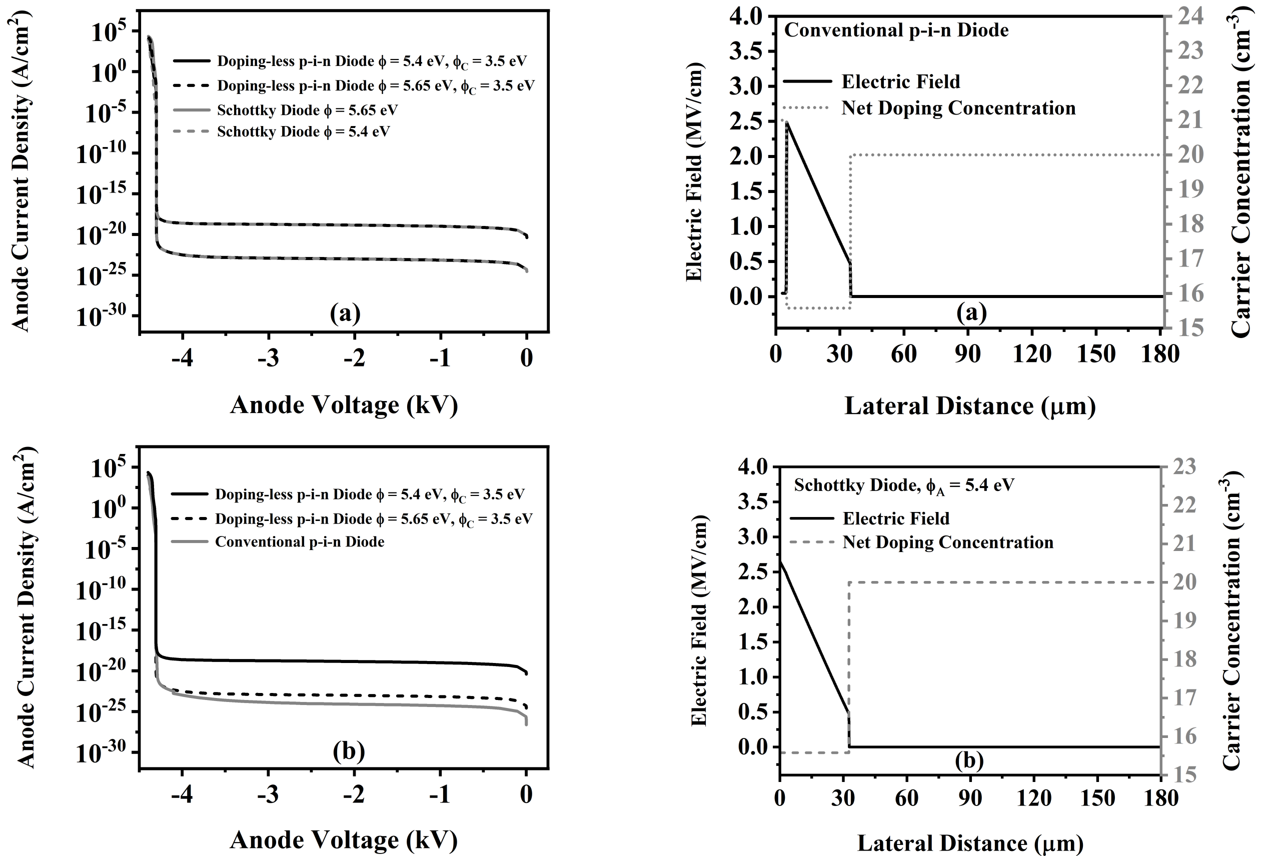

FIGURE 7. **(a) Semi-log reverse I-V characteristics of doping-less p-i-n diode and Schottky diode for two different anode electrode work-functions of 5.4 *eV* and 5.65 *eV*. (b) Semi-log reverse I-V characteristics of doping-less p-i-n diode for two different anode electrode work-functions of 5.4 *eV* and 5.65 *eV* and conventional p-i-n diode.**

and diffusion reverse saturation are the two contributors in the reverse saturation current (leakage current) [1]. Because Schottky diode and doping-less p-i-n diode have the same current mechanism, the reverse I-V characteristics of these two devices are almost identical. Fig. 7(b) distinctly demonstrates that as a result of the difference between current mechanisms of the Schottky barrier junction and the conventional p-n junction, the reverse saturation current density (leakage current density) of the doped p-i-n diode is at least an order of magnitude smaller than the leakage current density of the Schottky diode along with the doping-less p-i-n diode.

As it can be seen in Fig. 7(b) and later on in more details in Fig. 11, this variation between the current densities is prone to change as the work-function of the anode Schottky contact or temperature varies [1], [25]. Fig. 7 shows an increase in barrier height results in a lower leakage current in the Schottky diode, as well as doping-less p-i-n diode. In Schottky diode and doping-less p-i-n diode during reverse-bias, due to the applied negative voltage to anode Schottky metal with respect to semiconductor, the barrier height increases.

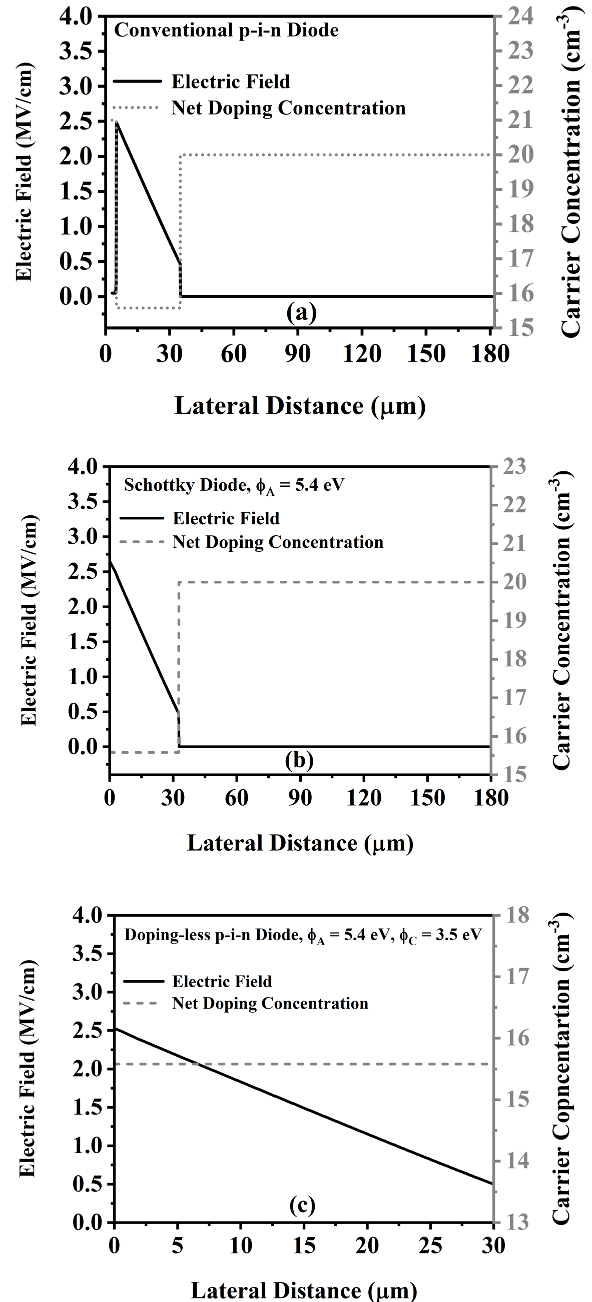

FIGURE 8. **(a) 1-D electric field and net doping profiles versus device depth in the doped p-i-n diode along a vertical cut-line. (b) 1-D electric field and net doping profiles versus depth in a Schottky diode along a vertical cut-line. (c) 1-D electric field and net doping profiles versus device depth in a doping-less p-i-n diode along a vertical cut-line.**

A lightly doped drift region in the Schottky diode and the doping-less p-i-n diode supports high blocking voltages. The drift region prevents the development of a sharp potential barrier by enabling the spread of the depletion region over a significant distance. The electric field profiles of the conventional p-i-n diode, the Schottky diode and, the doping-less p-i-n diode during breakdown, as well as their net doping profiles, are shown in Fig. 8.

Fig. 8(a) indicates the punch-through electric field profile of the doped p-i-n diode. Due to the parallel plane design of the conventional p-i-n diode, the maximum electric field of approximately 2.5 MV/cm is noticed at the anode/drift junction and gradually decreases towards the drift/cathode junction. The electric field remains high throughout the drift region, and its magnitude at the P and N regions is approximately zero.

Similarly, a punch-through electric field profile of the Schottky diode is presented in Fig. 8(b). The maximum electric field happens at the Schottky interface and remains high across the 30μm drift region. The electric field is degrading as we move away from the anode towards the cathode side, and it is approximately zero in the 150μm cathode region.

The doping-less p-i-n diode unlike the conventional p-i-n diode and Schottky diode does not have the thick 150μm N region to demonstrate the punch-through electric field, therefore the whole electric field profile as it is represented in Fig. 8(c), is across the entire 30μm doping-less p-i-n diode. The maximum electric field of approximately 2.5 MV/cm happens at the anode Schottky contact interface while it declines through the 30μm doping-less p-i-n diode, and the minimum electric field happens at the cathode contact and SiC interface.

Fig. 9 shows the forward and reverse characteristics of the doping-less p-i-n diode with two different cathode contacts work-functions of 3.5 eV and 3.9 eV. The cathode contacts are chosen in such a way so that they have a lower work-function than the SiC and create the negative induced charges at the interface. As it is mentioned before, the current mechanism of the doping-less p-i-n diode is determined by thermionic emission of the carriers through the barrier height created by the contacts with work-function greater than the SiC. Therefore, as long as the cathode contacts work-function remain below the work-function of the SiC to avoid the formation of the barrier height, the impact of the cathode work-function is negligible in forward and reverse characteristics of the device, as it is shown in Fig. 9.

B. TEMPERATURE DEPENDENCY

Temperature holds an important role in characterization of the semiconductor devices. Temperature fluctuation could be related to the power dissipation within devices in power circuits or changes in ambient temperature. Hence, it is crucial to assess the impact of temperature fluctuation on the performances of the semiconductor devices such as forward and reverse modes of operation. Fig. 6(a) shows the zoomed-in view of the linear forward characteristics of the conventional p-i-n diode. The ON-state voltage drop of the doped p-i-n diode decreases as the temperature rises from 300 K to 450 K [1].

The thermionic emission theory is utilized to characterize the current mechanism over the Schottky barrier in the

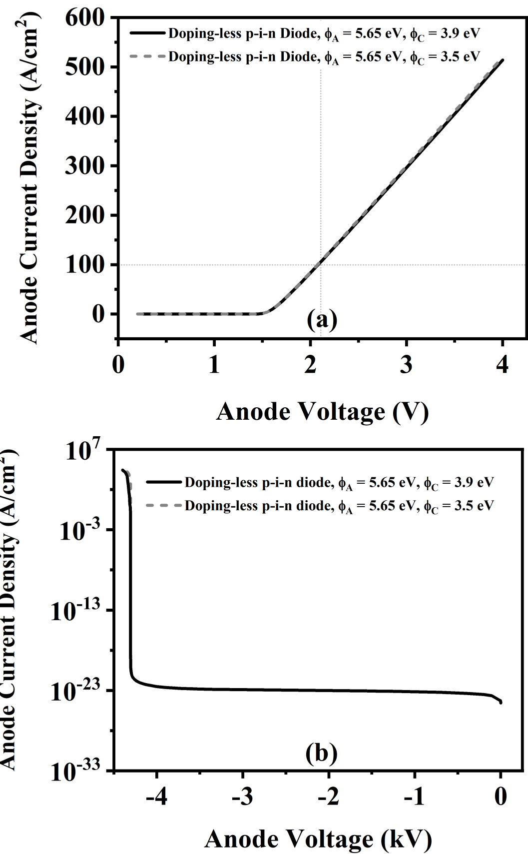

FIGURE 9. **(a) Forward I-V characteristics and (b) Reverse I-V characteristics of the doping-less p-i-n diode with two different cathode contacts with the work-functions of 3.5 eV and 3.9 eV.**

doping-less-p-i-n diode and the Schottky diode [1]:

$$J = A.T^2.e^{-q.\phi_b/k.T}.[e^{q.V/KT} - 1]\ A.cm^{-2} \tag{2}$$

where A is the effective Richardson's constant, T is the absolute temperature, k is the Boltzmann's constant, ϕ_b is the Schottky barrier height and V is the applied bias (positive and negative voltages). The value of effective Richardson's constant for SiC is 146 $A.cm^{-2}.K^{-2}$.

This equation can be considered for both forward (positive values for V in (2)) and reverse (negative values for V in (2)) biases. Under equilibrium condition (zero bias), it balances out the current from the metal and the semiconductor. By applying positive voltage, the second term in the equation comes to be negligible, with $A.T^2.e^{-q.\phi_b/k.T}$ being the saturation current density. As it can be observed temperature and barrier height have considerable effects on the saturation current density [1]. In the previous section, we already established the fact that the saturation current density of the Schottky diode and doping-less p-i-n diode increases with reduction of the work-function from 5.65 eV to 5.4 eV. Fig. 6(b) and Fig. 6(c) demonstrate, at 100 A/cm^2 forward current density, an increase in lattice temperature from 300 K to 450 K causes a steady increase in saturation current density and consequently in forward current density of Schottky diode as well as doping-less p-i-n diode.

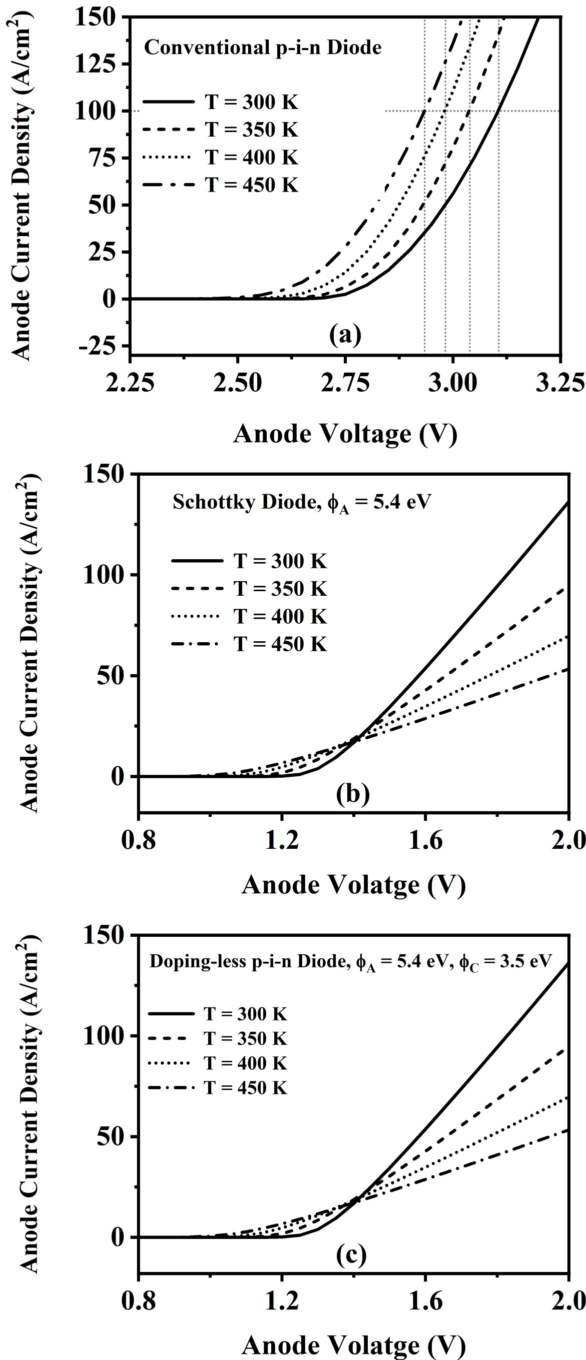

FIGURE 10. (a) Temperature dependency of the forward characteristics of the conventional p-i-n diode on a linear scale. (b) Temperature dependency of the forward characteristics of the Schottky diode on a linear scale. (c) Temperature dependency of the forward characteristics of the doping-less p-i-n diode on a linear scale.

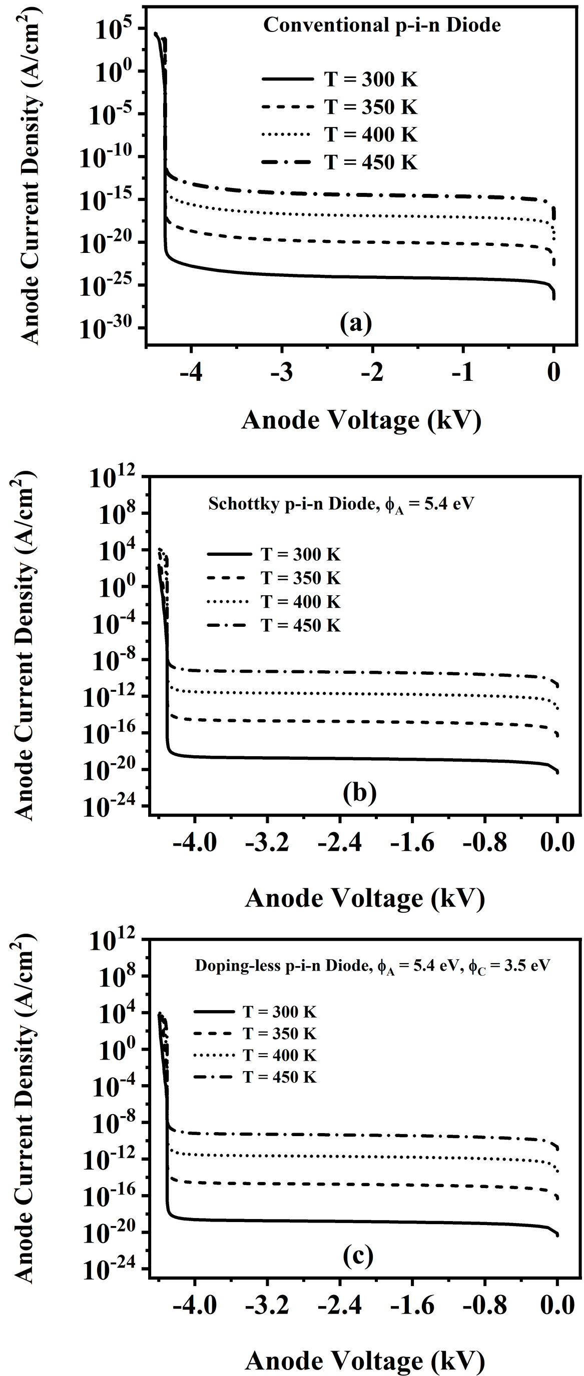

FIGURE 11. (a) Temperature dependency of the reverse characteristics of the conventional p-i-n diode on a linear scale. (b) Temperature dependency of the reverse characteristics of the Schottky diode on a linear scale. (c) Temperature dependency of the reverse characteristics of the doping-less p-i-n diode on a linear scale.

The voltage drop of the Schottky component can be approximated as below, at low forward current density [24]:

$$V_F \approx V_{Sch} = \phi_b + (k.T/q).\ln(J_F/A.T^2) \ \ V \tag{3}$$

As Fig. 6(b) and Fig. 6(c) indicate, based on (3) at low forward current density, the ON-state voltage drop decreases as the lattice temperature increases from 300 K to 450 K in Schottky diode as well as doping-less p-i-n diode [1], [24].

In terms of the reverse characteristics, in p-i-n diodes the total leakage current is given by:

$$J_L = \frac{q.D_n.n_i^2}{L_n.N_{AP+}} + \frac{q.(2d).n_i^2}{\tau_{sc}} + \frac{q.D_p.n_i^2}{L_n.N_{DN+}} \ \ A.cm^{-2} \tag{4}$$

where N_{AP+} and N_{DN+} are doping concentration in the P and N end regions, respectively. n_i is intrinsic carrier concentration and $2d$ is the width of the drift region. D_n and D_p are the diffusion coefficients for electrons and holes respectively, τ_{sc} is the space-charge region generation lifetime. L_n and L_p are diffusion lengths for electrons and holes, respectively.

The space-charge generation current is a dominant mechanism in the leakage current of the doped p-i-n diode and is susceptible to change as the temperature elevates. As Fig. 7(a) illustrates, the leakage current of the doped p-i-n diode rises as temperature increases [1].

The reverse saturation current for the Schottky diode and consequently doping-less p-i-n diode is obtained by substituting a negative value for V in (2). In (2), the thermal energy $(k.T/q)$ is much smaller than the applied reverse bias. Therefore, the first term in the bracket comes to be negligible in comparison to the second term. Hence, the leakage current is equal and opposite to the saturation current:

$$J = -A.T^2.e^{-q.\phi_b/k.T} \quad A.cm^{-2} \tag{5}$$

Fig. 7(b) and Fig. 7(c) indicate, by increasing the temperature from 300 K to 450 K, the saturation current density in the Schottky diode and the doping-less p-i-n diode increases, while the breakdown voltage remains stable.

IV. CONCLUSION

A novel 4200 V doping-less SiC p-i-n diode is designed for the first time using the charge plasma technique. The charge plasma process excludes the steps and high thermal budget during the fabrication process by considering metal electrodes with appropriate work-functions to create the P and N regions in a semiconductor. We have designed the doping-less p-i-n diode, with the specifications comparable to the conventional doped p-i-n diode and Schottky diode. The forward and reverse characteristics of the doping-less p-i-n diode and their response to elevated temperature are compared to the Schottky diode and conventional doped p-i-n diode. Because of the thermionic emission mechanism in the Schottky diode and doping-less p-i-n diode, the forward and reverse I-V characteristics of these two devices are almost identical. However, in comparison with the conventional p-i-n diode at ON-state current density of 100 A/cm^2, the doping-less p-i-n diode has a lower ON-state voltage drop, and during reverse bias, the doping-less p-i-n diode has a higher reverse saturation current.

Barrier height and temperature have significant impacts on the forward and reverse characteristics of the doping-less p-i-n diode. By increasing the barrier height (increasing the work-function of the anode electrode), the reverse saturation current of the doping-less p-i-n diode reduces while the ON-state voltage drop rises during forward bias.

As a result of increasing the temperature in conventional p-i-n diode, under forward bias, the ON-state voltage drop reduces, and during the reverse bias, the leakage current increases. Our results indicate that the forward and reverse I-V characteristics of the doping-less p-i-n diode has a consistent temperature dependency as the Schottky diode. During forward bias, at very low current densities, intensifying the temperate lessens the ON-state voltage drop in doping-less p-i-n diode. However, at higher forward current densities increasing the temperature gives a rise to the ON-state voltage drop. During the reverse bias, the reverse saturation current of the doping-less p-i-n diode increases with temperature in the same manner as the Schottky diode.

REFERENCES

[1] B. Baliga, *Fundamentals Power Semiconductor Devices*, New York, NY, USA: Springer, 2010.

[2] T. Kimoto and J. A. Cooper, *Fundamentals of Silicon Carbide Technology: Growth, Characterization, Devices and Applications*. Hoboken, NJ, USA: Wiley, 2014.

[3] R. J. E. Hueting, B. Rajasekharan, C. Salm, and J. Schmitz, "The charge plasma P-N diode," *IEEE Electron Device Lett.*, vol. 29, no. 12, pp. 1367–1369, Dec. 2008.

[4] B. Rajasekharan, J. E. Hueting, C. Salm, T. Hoang, and J. Schmitz, "Charge plasma diode—A novel device concept," in *Proc. 11th Annu. Workshop Semiconductor Adv. Future Electron. Sensors (SAFE)*, Dec. 2008, pp. 576–579.

[5] B. Rajasekharan, R. J. E. Hueting, C. Salm, T. van Hemert, R. A. M. Wolters, and J. Schmitz, "Fabrication and characterization of the charge-plasma diode," *IEEE Electron Device Lett.*, vol. 31, no. 6, pp. 528–530, Jun. 2010.

[6] K. Nadda and M. J. Kumar, "A novel doping-less bipolar transistor with Schottky collector," in *Proc. Int. Semiconductor Device Res. Symp. (ISDRS)*, Dec. 2011, pp. 1–2.

[7] M. J. Kumar and K. Nadda, "Bipolar charge-plasma transistor: A novel three terminal device," *IEEE Trans. Electron Devices*, vol. 59, no. 4, pp. 962–967, Apr. 2012.

[8] K. Nadda and M. J. Kumar, "Schottky collector bipolar transistor without impurity doped emitter and base: Design and performance," *IEEE Trans. Electron Devices*, vol. 60, no. 9, pp. 2956–2959, Sep. 2013.

[9] K. Nadda and M. J. Kumar, "Vertical bipolar charge plasma transistor with buried metal layer," *Sci. Rep.*, vol. 5, no. 1, pp. 1–6, Jan. 2015.

[10] A. Bansal and M. J. Kumar, "Investigation of laterally single-diffused metal oxide semiconductor (LSMOS) field effect transistor," *Current Appl. Phys.*, vol. 15, no. 10, pp. 1130–1133, Oct. 2015.

[11] P. Nautiyal, A. Naugarhiya, and S. Verma, "Application of workfunction engineering in vertical superjunction devices," *Superlattices Microstruct.*, vol. 109, pp. 927–935, Sep. 2017.

[12] S. Zafar, M. A. Raushan, S. Ahmad, and M. J. Siddiqui, "Reducing off-state leakage current in dopingless transistor employing dual metal drain," *Semicond. Sci. Technol.*, vol. 35, no. 1, Dec. 2019, Art. no. 015016.

[13] M. Gupta and A. Kranti, "Bi-directional junctionless transistor for logic and memory applications," *IEEE Trans. Electron Devices*, vol. 66, no. 10, pp. 4446–4452, Oct. 2019.

[14] M. J. Kumar, S. Hahmady, R. Gale, and S. Bayne, "Charge plasma high voltage pin diode investigation," in *Proc. IEEE Int. Power Modulator High Voltage Conf. (IPMHVC)*, Jun. 2018, pp. 117–121.

[15] S. Hahmady and S. Bayne, "Reverse recovery of 50 V silicon charge plasma PIN diode," *IEEE Access*, vol. 8, pp. 170588–170594, 2020.

[16] S. Ramaswamy and M. J. Kumar, "Junctionless impact ionization MOS: Proposal and investigation," *IEEE Trans. Electron Devices*, vol. 61, no. 12, pp. 4295–4298, Dec. 2014.

[17] F. Bashir, S. A. Loan, M. Rafat, A. R. M. Alamoud, and S. A. Abbasi, "A high performance gate engineered charge plasma based tunnel field effect transistor," *J. Comput. Electron.*, vol. 14, no. 2, pp. 477–485, Jun. 2015.

[18] M. J. Kumar and S. Janardhanan, "Doping-less tunnel field effect transistor: Design and investigation," *IEEE Trans. Electron Devices*, vol. 60, no. 10, pp. 3285–3290, Oct. 2013.

[19] S. Ramaswamy and M. J. Kumar, "Raised source/drain dopingless junctionless accumulation mode FET: Design and analysis," *IEEE Trans. Electron Devices*, vol. 63, no. 11, pp. 4185–4190, Nov. 2016.

[20] S. Chen, H. Liu, S. Wang, T. Han, W. Li, and X. Wang, "A novel Ge based overlapping gate dopingless tunnel FET with high performance," *Jpn. J. Appl. Phys.*, vol. 58, no. 10, Sep. 2019, Art. no. 100902.

[21] K. Kao and L. Chen, "A dopingless FET with metal–insulator–semiconductor contacts," *IEEE Electron Device Lett.*, vol. 38, no. 1, pp. 5–8, Nov. 2017.

[22] S. Sahay and M. J. Kumar, *Junctionless Field-Effect Transistors: Design, Modeling, and Simulation*, Hoboken, NJ, USA: Wiley, 2019.

[23] *ATLAS Device Simulation Software*, Santa Clara, CA, USA, Silvaco Int., 2012.

[24] B. N. Pushpakaran and S. B. Bayne, *Modeling and Electrothermal Simulation of SiC Power Devices*. Singapore: World Scientific, 2019.

[25] D. Neeman, *Semiconductor Physics and Devices*. New York, NY, USA: McGraw-Hill, 2012.

SARA HAHMADY received the B.S. degree in electrical engineering from Azad University, Iran, and the master's degree in VLSI design from the Indian Institute of Technology Delhi (IITD). She is currently pursuing the Ph.D. degree in electrical engineering with Texas Tech University. Her research interests are in semiconductor devices and fabrication.

STEPHEN BAYNE (Senior Member, IEEE) received the B.S., M.S., and Ph.D. degrees in electrical engineering from Texas Tech University. After completing his doctoral studies, he joined as an Electronics Engineer with the Naval Research Laboratory (NRL), where he design advanced power electronics systems for space power applications. After two and half years at NRL, he transferred to the Army Research Laboratory (ARL), where he was instrumental in developing the high-temperature silicon carbide power electronics program. He was promoted to a Team Lead at ARL, where he led the power components team which consisted of five engineers. As a Team Leader, he was responsible for advanced research in high-temperature and advance power semiconductor devices for army applications. After one and half years as a Team Lead, he was promoted to the Branch Chief of the Directed Energy Branch, where he managed 16 engineers, technicians, and support staff. He managed a multi-million-dollar budget and responsible for the recruitment, development, and performance evaluation of members in the branch. After eight years at the ARL, he transitioned over to academia, where he is currently a Professor with Texas Tech University. His research interests at Texas Tech are power electronics, power semiconductor devices, pulse power, and renewable energy. He is a Faculty Member of ARL South for the power and energy research at Texas Tech University. He has over 150 journal and conference publications. He is also a veteran of the military, where he served four years in the air force.